UVC-Based Biofouling Suppression for Long-Term Deployment of Underwater Cameras

Peter Adam Hoeher, *Fellow, IEEE*, Oliver Zenk, Boris Cisewski, Karin Boos, and Joachim Groeger

***Abstract*—Spatially distributed underwater sensor systems are important tools to understand long-term trends in marine ecosystems. For example, in the ongoing UFOTriNet project, noninvasive techniques for the purpose of monitoring fish populations are investigated. A challenge within this and related projects is the long-term operation of cameras in brackish and fully saline water. The impact of biofouling, especially on the underwater cameras, should be minimized for reliable imaging. In the context of the UFOTriNet project, for this purpose, an energy-efficient and environmentally friendly antifouling concept based on UVC irradiation was developed and investigated to extend operation times and to reduce energy and maintenance costs. Innovative contributions include LED-based UVC irradiation from the inside of the camera's pressure housing into the water column, periodic UVC irradiation intervals that are significantly shorter than those commonly reported, and an analysis and comparison of the irradiance for internal and external irradiation configurations. The concept was confirmed by a measurement campaign in the Kiel Fjord, located in the southwest Baltic Sea.**

***Index Terms*—Biofouling, long-term monitoring, UVC irradiation, underwater optics.**

I. Introduction

MARINE ecosystems are highly dynamic living systems that are continuously changing under the influence of a wide range of external factors. They mostly suffer from multiple pressures due to, e.g., fisheries, climate change, and discharges of pollutants as well as nutrients, and are thus, in the focus of UFOTriNet [underwater fish observatory (UFO)]. UFOTriNet is a multidisciplinary project for long term *in situ* sensing intended to monitor the status and dynamics of fish stocks in their complex ambient environment in the Bay of Kiel, Germany. As part of UFOTriNet, a trilateral test network of three different variants of UFOs is being developed: a stationary, a portable, and a mobile one, which are virtually connected to collect and analyze combined information using a wide range of sensors (see Fig. 1). Two of the core sensors being used in all three UFO variants are a stereo camera system and a sonar, the observations of which will be fused together based on artificial intelligence (AI) to provide estimates of fish abundance and biomass.

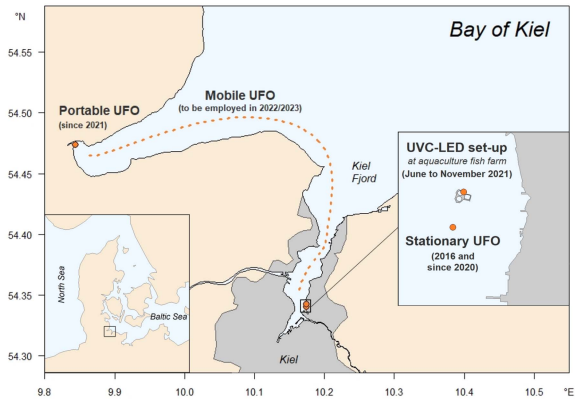

Fig. 1. Positions of the UFOTriNet stations in the Bay of Kiel, Germany. The map section on the right shows the location of the UVC-LED prototype, about 50 m away from the stationary UFO. The coastlines were determined with Google Earth Pro.

A similar project using a distributed network of underwater cameras for fish and environmental monitoring was recently described in [1]. Also related is the buoy-borne underwater imaging system presented in [2]. Yet another option is automatic underwater vehicle (AUV) swarms equipped with cameras and/or optical communication units [3], in conjunction with docking stations for long-term deployment.

While aiming to provide an automated, continuous, and noninvasive monitoring approach with UFOTriNet, one of the central problems of permanent underwater observations is the so-called biofouling, i.e., the colonization of structures by marine organisms such as microorganisms, plants, algae, and small animals (see also [4]). The barnacle *Balanus improvisus* (Darwin, 1854) and the blue mussel *Mytilus edulis* (Linnaeus, 1758), for example, are among the most common species found in epibenthic communities in the Baltic Sea [5], [6]. Showing high tolerances to a broad range of physical parameters, early life stage performance and settlement have been shown to be particularly affected by temperature, salinity, nutrient availability (typically

Manuscript received 26 June 2022; revised 21 March 2023; accepted 30 March 2023. This work was supported by the UFOTriNet project under Grant 2819111518 through the Federal Ministry of Food and Agriculture (BMEL) based on a decision of the Parliament of the Federal Republic of Germany via the Federal Office for Agriculture and Food (BLE) under the innovation support program. *(Corresponding author: Peter Adam Hoeher.)*

Associate Editor: B. Cochenour.

Peter Adam Hoeher is with the Faculty of Engineering, Kiel University, D-24143 Kiel, Germany, and also with the ComSupport GbR, D-24226 Heikendorf, Germany (e-mail: ph@tf.uni-kiel.de).

Oliver Zenk is with the MacArtney Germany GmbH, D-24148 Kiel, Germany (e-mail: oze@macartney.com).

Boris Cisewski and Karin Boos are with the Thuenen Institute of Sea Fisheries, D-27572 Bremerhaven, Germany (e-mail: boris.cisewski@thuenen.de; karin.boos@thuenen.de).

Joachim Groeger is with the GEOMAR Helmholtz Centre, D-24148 Kiel, Germany, and also with the Thuenen Institute of Sea Fisheries, D-27572 Bremerhaven, Germany (e-mail: groeger@geomar.de).

Digital Object Identifier 10.1109/JOE.2023.3265164

Fig. 2. (a) Deployment of the stationary UFO with clean and untreated surfaces in Kiel Fjord in April 2016 and (b) its retrieval 24 weeks later. The weight difference due to overgrowth by mostly barnacles and mussels was approximately 500 kg given an initial weight of 350 kg, i.e., the mass was more than doubled. Close ups: (c) Stereo-camera of the stationary UFO in frontal view in the clean and untreated status and (d) after its retrieval. The black arrow in (c) indicates the arm of the wiper, which, when in operation brushes over the glass fronts of the two cameras. The white arrows in (d) point to various life stages of the blue mussel *Mytilus edulis* settling on available UFO-surfaces.

expressed as chlorophyll as a proxy for planktonic feed), and water velocity (see [7], [8], and references therein). Especially in the summer months, available structures for settlement may be rapidly overgrown and may not only affect the functioning of the sensors but also add considerably to the total weight, making retrieval operations a serious challenge (see Fig. 2).

Biofouling can cause functional and structural deficiencies. Often discussed is the influence of biofouling on the frictional resistance of ships' hulls and the effect on underwater sensors, less frequently, the influence on optical devices. For opaque surfaces, fouling control is considered successful, for example, as long as a sensor does not fail in the presence of residual fouling, or the frictional resistance of the hull is below a certain level. However, for transparent surfaces, the situation is different. In the case of underwater camera systems, additional limitations apply. First, even a single mussel or barnacle settling on the glass front of the camera, subsequently called the camera window or optical window, would degrade image quality. Second, image quality should not be degraded by anti-biofouling technology.

A. Motivation and Goals

Stationary long-term monitoring systems for oceanic habitats suffer particularly from biofouling. As the degradation through biofouling also affects camera windows, which need to be cleaned constantly, to allow for clear and unbiased underwater video imaging, extended operation times, and reducing the maintenance costs. The mechanically susceptible and energy-intensive wiper used so far in the UFOTriNet project to clean the camera windows, depicted in Fig. 2, is intended to be replaced or at least complemented by an effective, low-energy, and environmentally friendly antifouling tool. Among the favorable solutions is irradiation with short-wave ultraviolet (UVC) light employing light emitting diodes (LEDs). For an introduction to UV-based biofouling protection, see [9].

The focus of this article is on UVC-LED-based biofouling suppression for underwater camera glass fronts. The goal of this irradiation method is to prevent the adhesion of larvae, especially from mussels and barnacles. UVC light at wavelengths of about 250–280 nm is capable of altering DNA in such a way that this process is largely avoided. The peak of the wavelength-dependent inactivation of microbes occurs at about 265 nm [10]. However, mussels and barnacles that are already attached to a surface cannot be removed by subsequent irradiation. In this respect, the main objective of anti-biofouling techniques for camera systems is to almost completely suppress the adhesion of larvae from the start and over the entire period of use, to guarantee high quality imaging. This distinguishes our work from UVC-based anti-biofouling projects for nontransparent surfaces. Special interest is given to energy savings in mobile and portable devices.

B. State-of-The-Art

Numerous antifouling techniques have been developed. A selection of passive and active techniques suitable for transparent surfaces is reported next. They can be combined with UVC irradiation. For further current trends see [11] and [12].

1) Mechanical treatment: Mechanical methods such as wipers [13], [14], [15] and cleaning robots [16] are able to remove any sort of biofouling organisms on flat surfaces including glass. Disadvantages include high peak power (during activation phases), mechanical stress on the wiper/robot in heavy seas, and the risk of scratching optical windows.
2) Antifouling paints: Organotin antifouling paints such as tributyltin (TBT) effectively reduce biofouling, but are toxic and therefore are banned worldwide. Biocide-free antifouling coatings have been available since the mid-1990s [13], [14], [17], [18]. Antifouling coatings are currently the most popular method for ships' hulls, underwater gliders, and large-scale underwater installations. Most antifouling paints are not transparent, however, transparent coatings have also been developed [19]. Although the antiwetting properties of the initially proposed transparent coatings were either toxic or fading after submergence in seawater [17], while coatings suitable for underwater cameras and optical instrumentation are reported to last for a few months [15].
3) Nano and foil coatings: Sprayable nano coatings with a long service life [20], [21] as well as foil coatings [22]

represent an environmentally friendly alternative to classic anti-fouling paints. Like antifouling paints, most nano coatings are not transparent and therefore not suitable for underwater cameras. Still, some transparent nano coatings have been developed and tested on glass surfaces, see, for example, [23], [24], but sometimes their biofouling protection is time-limited or sometimes they are not transparent in the ultraviolet range, although they are transparent in the visible range.

4) Local chlorination: A typical configuration of local chlorination [25] is the use of a housing or enclosure that encapsulates the sensors to be protected [14]. A chlorine solution is injected into the sensor area to extend the duration of use. Liquid sterilization systems achieve an effective duration of several months. An application to underwater optical windows has recently been published [26].
5) Copper plates/bezels: For moored optical sensors, copper can effectively replace chemical antifoulant methods, as demonstrated for open, enclosed, semienclosed, and shuttered optical instrumentation [15], [27].
6) Ultrasound: The cleaning effect of ultrasonic systems is based on the induction of cavitation [28]. The effect is achieved by the generation of microbubbles, which are created when a sufficiently high negative pressure is applied to a liquid. Compression and decompression waves pass through the fluid very quickly. If the waves are sufficiently strong, the gas bubbles generated will increase in size until they implode [29]. The collapse of the gas bubbles produces a rapid and extreme rise in temperature as well as pressure, both of which cause the generation of free radicals with strong oxidative properties. A study on ultrasonic waves to suppress biofouling on an optical surface was recently published [30]. Still, the use and benefits of ultrasonic systems as a fouling protection technique are discussed controversially [31].
7) Electric fields: Alternating electric fields are used industrially to reduce fouling in heat exchangers. According to Faraday's law, an oscillating electric field provides the necessary molecular motion to dissolve mineral ions. In the field of marine fouling, this principle can also be applied [32], [33]. The comparatively few results published so far are promising.
8) Laser irradiation: Biofouling removal from marine surfaces using a laser is another novel technology [34]. The aim is to achieve lethal damage to microorganisms and their cell compounds by laser radiation, and then to achieve a cleaning effect by water flow. This technology has similarities with ultraviolet germicidal irradiation. Very high intensities per square millimeter are achievable, however, the positioning of the laser beam is complicated. The latter task is not necessary when UV LEDs with a sufficiently large beamwidth are used.
9) Ultraviolet germicidal irradiation: Ultraviolet germicidal irradiation [10] is a disinfection method that uses shortwave ultraviolet light to inactivate microorganisms such as viruses and bacteria or small organisms including larvae by altering their DNA, so that they can no longer perform vital functions. UV irradiation is used in a variety of applications, like cleaning/disinfection of surfaces (surgical instruments, sterile rooms, etc.), food, air, and (waste) water. The effects of UV radiation at different wavelengths on marine macrobenthic communities have been studied extensively, see e.g., [35], [36], [37], [38], [39].

In the context of underwater biofouling prevention, the method of UV irradiation has been well researched for a long time [40]. In the early beginnings, 250 W low-pressure mercury vapor lamps were used, which later were replaced with 5–10 W lamps [41]. Low-pressure mercury vapor lamps are characterized by a strong emission line at 253.8 nm. Subsequently, polychromatic ultraviolet irradiation with medium-pressure mercury vapor lamps was also investigated [42], before UV LEDs became available.

In almost all publications to date, nontransparent surfaces are considered, yet this noncontact method is well suited also for underwater cameras, both for flat optical ports and dome ports. To the best knowledge of the authors, UV-based fouling control for underwater optical devices has been reported in only two early journal papers: DiSalvo et al. [41] studied marine antifouling effects for a pressure housing equipped with a quartz window. Continuous irradiation was performed from the outside of the housing, the inside of the housing, and a polished side face of the optical window. Patil et al. [43] mounted glass plates in test coupon holders and submerged them in a pond without using a waterproof enclosure. The glass plates were irradiated with different intensities and exposure times. In both articles, mercury vapor lamps were used.

Various studies using UV LEDs for disinfection and sterilization in various fields have been reported since 2007 [44], [45]. UV LEDs are small and lightweight, are suitable for mobile use, allow freedom in the design of radiator modules, offer the possibility of UVA/B/C wavelength selection, provide narrowband emission almost without spurious peaks, do not require an electronic ballast for starting, are functional without preheating, operate at low direct current (dc) voltages and currents, can be switched ON and OFF fast, are maintenance free, and do not contain toxic materials like mercury. The radiation intensity can be easily adjusted electrically. As the heat dissipation in the emission direction is small, the environmental impact caused by heat is negligible. The service life of semiconductor LEDs is improved by periodically switching them ON and OFF. Nevertheless, wall-plug efficiency and durability are subject to improvement. Initially, only long-wave ultraviolet (UVA) LEDs at about 365 nm were available and these were used in continuous mode for biofouling reduction. Meanwhile, a variety of effects have been studied for opaque surfaces, including the effects of wavelength (UVA, UVB, UVC), UV intensity, irradiation patterns, exposure time, and surface color. The following is a brief overview (in historical order) on recent contributions to marine biofouling control.

Bueley et al. [9] have focused on the design issues of an LED-based irradiation device and on *in situ* trials of UVC as an antifoulant to reduce biofouling induced measurement errors in underwater sensor systems. Salters et al. [46] presented a novel concept in which an array of UVC LEDs is mounted on a surface

such as a ships' hull. This LED array emits light outward from the surface and acts like a coating. Hunsucker et al. [47] aimed to determine whether the addition of UVC light could work in synergy with coatings on ships' hulls to enhance their performance. The study addressed coating types, frequency of UVC exposures, and influence of distance. MacKenzie et al. [48] investigated the effects of periodic UVC illumination on marine macrofouling by testing several UV illumination duty cycles against samples with no illumination. The variation of UV intensity, exposure time, and distance was examined by Ryan et al. [49]. Braga et al. [50] investigated a novel arrangement of UVC illuminants in the form of a nautilus. Richard et al. [51] studied the application of UVC used in synergy with surface materials. Particularly, the effect of surface color, reflectance, and exposure intervals (weekly intervals and 10 min intervals) were tested. Recently, Whitworth et al. [52] investigated the effect of duty cycles, durations, high and low dosages, and voltages for an LED array with emphasis on ships' hulls.

Apart from those research articles, numerous patents on UV-based irradiation for oceanic applications exist [53], [54], [55], [56], [57].

To the best of the authors' knowledge, no commercial UV-based biofouling suppression product designed for underwater cameras is currently available. For most commercial UV products, irradiation is through the water column, with the exception of a fluorometer series offered by Chelsea Technologies [12]. The UV.Xchange product from AML Oceanograpic, Ltd. was developed for outside irradiation of objects like underwater sensors [9], [58]. For similar applications, an anti-biofouling system was developed at the Leibniz Institute for Baltic Sea Research (IOW), which was certified only recently [59], and meanwhile produced by Mariscope under license from IOW. AkzoNobel, in cooperation with Royal Philips, announced LED-based cleaning of ships' hulls, propellers, and steering gears, related to the work in [46], [47], [51], and [52].

C. Innovative Contributions and Outline of the Article

Innovative contributions of this article include the following aspects.

1) LED-based UVC irradiation is from the inside of a camera's pressure housing into the water column.
2) Analysis and comparison of the irradiance for internal and external UV irradiation configurations.
3) Study of periodic irradiation intervals that are significantly shorter (and hence more seamless) than those commonly used.
4) Experimental verification in the urban Kiel Fjord, southwest Baltic Sea.

The rest of this article is organized as follows. In Section II, two different UVC irradiation scenarios are compared, an analysis of the irradiance is provided, and the proposed UVC irradiation design is introduced. In Section III, lab results as well as results of a measurement campaign in the Kiel Fjord are reported, supported by a statistical analysis. Afterward, the main findings are discussed in Section IV. Finally, Section V concludes this article.

II. Materials and Methods

A. UVC Irradiation Configurations

Irradiation of underwater windows can be carried out from three positions: exterior to the window, from behind the window, and from the side face(s) of the window(s) [41]. The first two options are illustrated in Fig. 3.

The advantages and disadvantages of both concepts are as follows.

1) External irradiation: In this concept, not only the optical window is irradiated, but also parts of the camera body. This feature is advantageous because larvae prefer to settle in bulges [14]. The risk of barnacles and mussels settling at the sides of the optical window is significantly reduced with this variant. Another advantage is that any type of glass can be used for the optical window, like borosilicate glass. Care must be taken to ensure that the irradiation fixture is located outside the field-of-view of the camera. For this purpose, a holder must be constructed that is subject to mechanical stress. The UV LED should preferably be encapsulated in a pressure-neutral manner [3], [55]. Still, the UV LED must be protected by quartz glass. The heat loss can be dissipated via the water without any problems. However, the power supply driving the UV LED must be routed to the outside.
2) Internal irradiation: In this concept, the optical window is irradiated from the inside. A mayor advantage is that attenuation caused by the water column is fully eliminated and turbidity is not an issue. For UV light, the attenuation is particularly strong. The mechanical construction remains compact and the slant range through the air can be made small, still avoiding that the irradiation fixture is within the field-of-view of the camera. No external holder is required, and the power supply driving the UV LED does not have to be routed to the outside. Among the disadvantages in low-cost implementations is that quartz glass must be used for the optical window. Care must be taken to ensure that the heat dissipation of the UV LED functions properly.

Irradiation from the side face(s) of the optical window, not illustrated in Fig. 3, is feasible only for polished edges. This promising concept is subject for future investigation.

B. Analysis of Irradiance

The germinating effect of UVC radiation depends on the dose (in joule per square meter) and the wavelength used (in nm). The dose is determined by the irradiance (in watts per square meter) and the effective duration of absorption (in seconds). The effectiveness of the germicidal action is wavelength-dependent with a maximum around 265 nm [10], making the germicidal effectiveness of commercial UVC LEDs greater than that of low-pressure mercury vapor lamps with a spectral line at 253.8 nm.

The light *dose* is calculated from the irradiance E_e, the absorption time T, and the duty cycle δ, according to

$$\text{dose} = E_\mathrm{e} \cdot T \cdot \delta. \tag{1}$$

The *dose rate* is the dose absorbed per unit time.

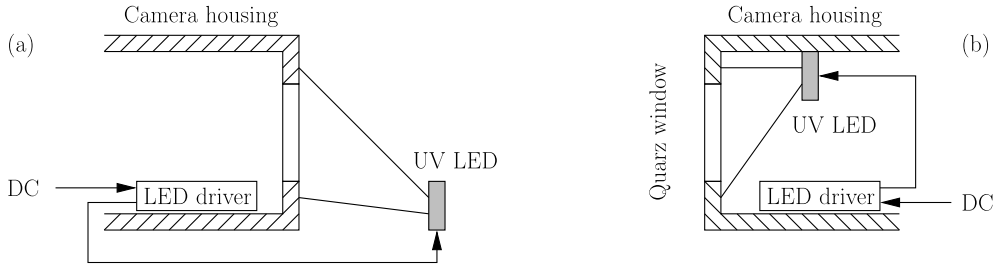

Fig. 3. LED-based UV irradiation configurations for underwater cameras. The UV LED can be mounted outside or inside the camera housing, see (a) for external irradiation and (b) for internal irradiation. Irradiation from the inside works only if the optical window is transparent to UV radiation. Fused silica is suitable for this purpose. UV LED and LED driver unit are not to scale in this sketch.

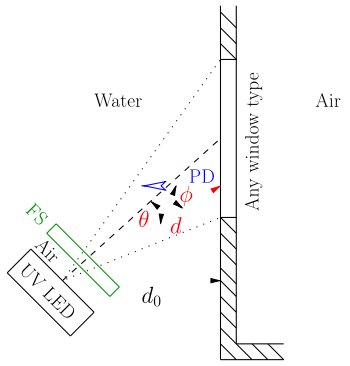

Fig. 4. Setup and notation for calculation of the irradiance for the case of external irradiation. The angles of irradiance and incidence are θ and ϕ, respectively. The fused silica (FS) glass depicted in the figure protects the UV LED from seawater.

Subsequently, we assume that the UV LED is either switched ON or switched OFF—this is a preferred mode of operation for semiconductor light sources. Then, the duty cycle δ ($0 < \delta \leq 1$) is defined as the ratio between the ON-time divided by the ON-plus-OFF-time. The product $T \cdot \delta$ can be interpreted as the effective absorption time, which is reduced by the duty cycle. The absorption time T should not be confused with the time of exposure, i.e., the duration of the experiment, which may last for some weeks or months. Rather, it is the effective time in which an object (such as a virus) is irradiated. As such, T is a random variable. For this reason, for a fair comparison of different irradiation schemes, it is more useful to consider the irradiance as an evaluation criterion, albeit the germinating effect is clearly determined by the dose.

The *irradiance* E_e is derived in the following for the two scenarios (a) and (b) introduced in Fig. 3. The irradiance is often expressed in W/m^2 or in μW/cm^2. The conversion from W/m^2 to μW/cm^2 is: 1 W/m^2 = 100 μW/cm^2.

1) External Irradiation: Let the UV LED be mounted at a vertical distance d_0 from the optical window plane (outside the field-of-view of the camera). The UV LED is assumed to be a point source, and aligned to the center of the optical window (see Fig. 4).

Each light irradiation device has a certain directivity. For a generalized Lambertian light source, the radiant intensity $I_\mathrm{e}(\theta)$ is a function of the angle of irradiance θ according to

$$I_\mathrm{e}(\theta) = I_\mathrm{e}(0) \cdot \frac{m+1}{2} \cos^m(\theta) \tag{2}$$

where $I_\mathrm{e}(0)$ is the light intensity in the boresight direction and

$$m = -\frac{1}{\log_2(\cos(\theta_{1/2}))} \tag{3}$$

is the so-called mode number. The mode number m depends on the half-power angle $\theta_{1/2}$ of the light source. For isotropic emitters (in the half-plane) $\theta_{1/2} = \pm 90°$ holds ($m = 0$), diffuse sources are obtained for $\theta_{1/2} = \pm 60°$ ($m = 1$), and directional spot beams are characterized by $\theta_{1/2} < \pm 60°$ ($m > 1$). For some commercial UV LEDs $\theta_{1/2} \approx \pm 60°$ is valid, for others (including the finally selected UV LED) not. For this reason, in the following:

$$I_\mathrm{e}(\theta) = I_\mathrm{e}(0) \cdot f(\theta) \tag{4}$$

the general relation is used, which holds for any rotationally symmetric intensity distribution. The influence of reflectors and/or lenses, if applied, can be taken into account in $f(\theta)$.

Let the slant range between the light source and some point on the optical window mounted in the pressure housing be denoted as d. Consequently, for the angle of incidence ϕ, the relation $\cos(\phi) = d_0/d$ holds. The distance must be much larger than the dimension of the UV LED for it to be interpreted as a point source. Let us assume a fictitious photodetector (PD) with area A_R placed on the water-side surface of the optical window. This window does not have to be UV transparent in the case of external irradiation, frequently borosilicate glass is used. Furthermore, let us assume that the UV LED is protected by a fused silica (FS) quartz window against seawater, dubbed the protection window. FS is a quartz glass consisting of almost pure silicon dioxide in amorphous (i.e., noncrystalline) form, characterized by a high transmittance of UVC light [60].

In air, the photodetector measures the optical received power (in W)

$$P_\mathrm{R} = \Phi_\mathrm{e}\, f(\theta)\, T_\mathrm{FS}(\phi)\, \frac{A_\mathrm{R} \cos(\phi)}{\pi d^2} \tag{5}$$

where $\Phi_\mathrm{e} = P_\mathrm{T}$ is the radiant flux (in W) and $T_\mathrm{FS}(\phi)$ is the transmission coefficient of the fused silica window at angle ϕ ($0 \leq T_\mathrm{FS}(\phi) \leq T_\mathrm{FS}(0) \leq 1$). The radiant flux depends on the UV LED type and on dimming. The transmission coefficient is a measure of how much of the UV light wave passes through the quartz window, i.e., the ratio of received powers with and without window. The transmission coefficient as defined here includes absorption inside the window (which is a function of glass type, wavelength, and path length in the glass), as well as

the Fresnel reflection loss at both window surfaces (which is a function of angle of incidence and material-dependent as well as wavelength-dependent refraction indices of the glass and its neighboring media). We will explore the transmission coefficient shortly.

Notice that $A_\mathrm{R}\,\cos(\phi)$ is the effective area of the photodetector. By definition, the irradiance E_e (in W/m^2) is equal to the received power per unit area. Thus, if the light source is switched ON

$$E_\mathrm{e} = \frac{P_\mathrm{R}}{A_\mathrm{R}} = \Phi_\mathrm{e}\, f(\theta)\, T_\mathrm{FS}(\phi)\, \frac{\cos(\phi)}{\pi d^2} \tag{6}$$

applies.

In seawater, an additional attenuation occurs, which according to the Beer–Lambert law is modeled by an exponential term, see, for example [3], [61], and [62]

$$E_\mathrm{e} = \Phi_\mathrm{e}\, f(\theta)\, T_\mathrm{FS}(\phi)\, \frac{\cos(\phi)}{\pi d^2}\, e^{-K\,d}. \tag{7}$$

The so-called diffuse attenuation coefficient for irradiance K, mainly depends on the type of water. In shallow and brackish waters, where biofouling control is of utmost interest, a relatively large attenuation coefficient K can be expected for short-wave UV emission [61], [62].

Now, we are ready to calculate the transmission coefficient $T_\mathrm{FS}(\phi)$. Let $n_1 = 1$, n_2, n_3 denote the refractive indices of air, quartz glass, and water, respectively. Reflection occurs at both window surfaces if $n_1 \neq n_2$ and $n_2 \neq n_3$. At 272 nm for instance, the refractive index of FS quartz glass is about $n_2 = 1.50$ [60] and the refractive index of seawater about $n_3 = 1.36$ (rounded to two decimal places). According to Snell's law [63]

$$\frac{\sin(\phi_1)}{\sin(\phi_2)} = \frac{n_2}{n_1} \quad \text{and} \quad \frac{\sin(\phi_2)}{\sin(\phi_3)} = \frac{n_3}{n_2} \tag{8}$$

for a given angle of incidence $\phi_1 = \phi$, one yields

$$\phi_2 = \sin^{-1}\left(\frac{n_1}{n_2}\sin(\phi_1)\right) \text{ and } \phi_3 = \sin^{-1}\left(\frac{n_2}{n_3}\sin(\phi_2)\right). \tag{9}$$

Unpolarized light can be decomposed into two components that are polarized perpendicular and parallel to the plane of incidence, respectively. The corresponding reflection coefficients are [63]

$$R_{12}^{\perp} = \left(\frac{n_1\cos(\phi_1) - n_2\cos(\phi_2)}{n_1\cos(\phi_1) + n_2\cos(\phi_2)}\right)^2$$
$$R_{12}^{\parallel} = \left(\frac{n_2\cos(\phi_1) - n_1\cos(\phi_2)}{n_2\cos(\phi_1) + n_1\cos(\phi_2)}\right)^2 \tag{10}$$

for the air-window interface, and

$$R_{23}^{\perp} = \left(\frac{n_2\cos(\phi_2) - n_3\cos(\phi_3)}{n_2\cos(\phi_2) + n_3\cos(\phi_3)}\right)^2$$
$$R_{23}^{\parallel} = \left(\frac{n_3\cos(\phi_2) - n_2\cos(\phi_3)}{n_3\cos(\phi_2) + n_2\cos(\phi_3)}\right)^2 \tag{11}$$

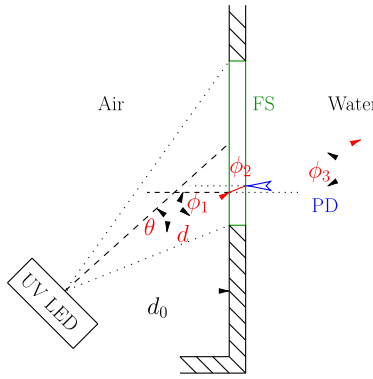

Fig. 5. Setup and notation for calculation of the irradiance for the case of internal irradiation.

for the window-water interface. The associated transmission coefficients are

$$T_{12} = 1 - \frac{R_{12}^{\perp} + R_{12}^{\parallel}}{2} \text{ and } T_{23} = 1 - \frac{R_{23}^{\perp} + R_{23}^{\parallel}}{2}. \tag{12}$$

Overall

$$T_\mathrm{FS}(\phi) = T_\mathrm{absorption}(\phi) \cdot T_{12} \cdot T_{23}. \tag{13}$$

For thin glass, the reflection loss dominates. The transmission coefficient decreases monotonically with $|\phi|$, i.e., for $\phi = 0$ the transmission through the window is maximized. For external irradiation, this optimum case is obtained when the protective window is mounted perpendicular to the target direction. Then, at an appropriate distance d, the beam is not noticeably refracted at both surfaces of the protective window. For $\phi = 0$, about 4% of the light intensity is reflected at the air-window interface and about 0.24% at the window-water interface.

2) Internal Irradiation: Regarding the calculation of the irradiance for the case of internal irradiation, the setup is shown in Fig. 5. As opposed to external irradiation, the UV LED does not need to be protected. This time, however, the optical window mounted in the pressure housing has an influence on the UV irradiation and therefore must be made of quartz glass. As for external irradiation, also for internal irradiation the irradiance can be expressed by (6) and the transmission coefficient by (13). Transmission is maximized when irradiation is perpendicular to the window plane, as has been done in our experiments. Still, the analysis applies for arbitrary angles of incidence.

3) Comparison of External and Internal Irradiation: It has already been mentioned that the dose is a random variable, because for larvae, the absorption time is randomly distributed. In contrast, for internal as well as external irradiation, the irradiance can be calculated for any point near the water-side surface of the optical window, provided the irradiance is measured by a photodetector pointing in a known direction (modeled by the effective area $A_\mathrm{R}\,\cos(\phi)$). In practice, however, the irradiance is also a random variable because the effective surface area of larvae, their orientation, and their distance to the optical window are randomly distributed.

If we compare the internal configuration, (6), with the outside configuration, (7), the influence of the water column is removed

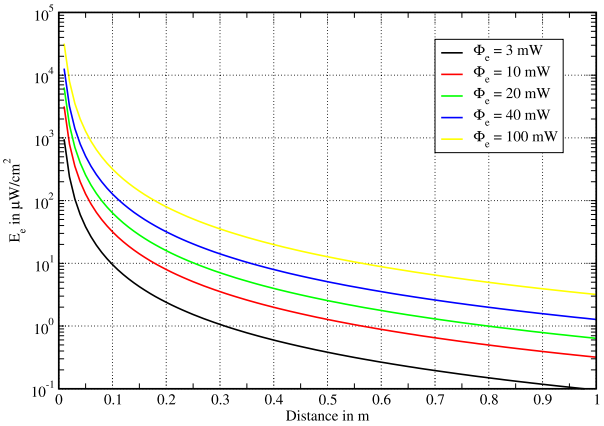

Fig. 6. Irradiance E_e as a function of distance d for different radiation fluxes Φ_e in air ($K = 0$, $T_\mathrm{FS}(0) = 1$). This situation applies for internal irradiation.

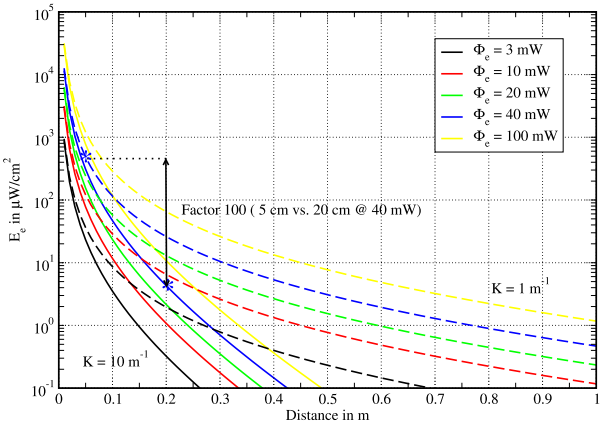

Fig. 7. Irradiance E_e as a function of distance d for different radiation fluxes Φ_e in water ($K = 1\,\mathrm{m}^{-1}$ and $K = 10\,\mathrm{m}^{-1}$, $T_\mathrm{FS}(0) = 1$). This situation applies for external irradiation.

for the internal configuration ($K = 0$). The effect is enhanced if the UV LED is positioned closer to the optical window for structural reasons. Although a protective glass in front of the UV LED can be avoided in the case of irradiation from the inside, the UV light is partially absorbed and reflected by the optical window, because fouling control is to be achieved on the water-side glass plane. The transmission coefficient $T_\mathrm{FS}(\phi)$ is therefore preserved. For fused silica, the transmission coefficient exceeds 90% in the wavelength region of interest at $\phi = 0$.

Figs. 6 and 7 show the irradiance E_e for internal irradiation (in air) and for external irradiation (in water), respectively. Both figures have in common that the UV LED is located at a distance $d = d_0$ perpendicular to the center of the optical window to be irradiated ($\phi = 0$). The irradiance is depicted as a function of the distance d assuming $T_\mathrm{FS}(0) = 1$. For Baltic Sea waters, an attenuation coefficient between $K = 1\ \mathrm{m}^{-1}$ (dashed lines) and $K = 10\ \mathrm{m}^{-1}$ (straight lines) can be expected, as extrapolated from [61].

For $\Phi_\mathrm{e} = 40$ mW (e.g., a 100 mW UV LED, dimmed to 40%), at a distance of 50 mm, $E_\mathrm{e} = 509\,\mu\mathrm{W/cm}^2$ is yielded in air. These parameters hold in the experimental setup reported subsequently when the UV LED was placed inside. For the same radiant flux, at a distance of 20 cm, the irradiance is only $E_\mathrm{e} \approx 4\,\mu\mathrm{W/cm}^2$ in water at $K = 10\ \mathrm{m}^{-1}$. This corresponds to an optical power loss of the order 100, i.e., two orders of magnitude. This value can be about expected for an outside arrangement and coincides with an observation made in [41]. In other words: the internal configuration is an important recipe for power savings in mobile and portable devices/systems.

C. UVC Irradiation Design

1) UV LED Selection: The following criteria for selecting UV LEDs should be considered: peak wavelength λ_peak, radiant flux Φ_e, wall-plug efficiency η_e, half-power angle $\pm\theta_{1/2}$, pressure resistance, power supply (I_F, V_F), and off-the-shelf availability. A product research revealed the commercial products listed in Table I.

For our underwater experiments, the 100 mW 272 nm UV LED offered by Bolb Inc. was selected (S6060-DR250-W275-P100-V6.5). The peak wavelength of 272 nm is close to the optimum wavelength of about 265 nm reported in [10] for microbes. The dimensions are 6.0×6.0 mm (6060 SMD package), which allows for many design possibilities. The wall-plug efficiency $\eta_\mathrm{e} = \Phi_\mathrm{e}/P_\mathrm{e} = \Phi_\mathrm{e}/(I_\mathrm{F} \cdot V_\mathrm{F})$ is just 6%–7%, but better than concurrent products offered at that time [64]. Currently, among the problems of UVC LEDs is aging [65]. In the September 2021 datasheet, the 70% lifetime (L70) is specified with 3000 h, and the 50% lifetime (L50) is reported as 5000 h for continuous operation. This means that after 3000 h (or 5000 h), the intensity typically drops to 70% (or 50%) of the initial intensity. This low lifetime compared to LEDs in the visible range is one of the reasons why the forward current I_F and the duty cycle δ were reduced in our experiments as explained next.

2) UV LED Driver Unit: LEDs should be current-controlled because small voltage fluctuations cause large current fluctuations according to Shockley's diode equation. Forward currents above the specified maximum current have a negative effect on the lifetime. In the specific application of an anti-biofouling device, a constant current source is even more important, because the radiant flux (i.e., the emitted optical power) is proportional to the forward current I_F of the diode. Current control is therefore important for reproducible measurements.

In this project, a UV LED driver unit was designed for multiple purposes: 1) electrical and optical power savings; 2) UV LED lifetime extension; and 3) dose rate adjustment by current control. The UV LED driver unit consists of two boards: a custom-made analogue driver circuit and an Arduino Nano microcontroller. By means of the LED driver board depicted in Fig. 8, the maximum radiant flux (in continuous UV emission mode) is adjustable. For example, the 100 mW optical power reported in the first row of Table I is reduced to 40 mW by reducing I_F from 250 to 100 mA. By means of the microcontroller, the duty cycle is adjustable via software code. The duty cycle δ is the ratio between on time and ON-plus-OFF time. Given a duty cycle of 10% for instance, the optical power and the forward current will be further reduced by a factor of ten. The average current consumption per LED is thus about 10 mA when the duty cycle is equal to 10%. In other words, analogue as well as digital

TABLE I
PRODUCT RESEARCH ON UVC LEDS IN ALPHABETICAL ORDER (AS OF DECEMBER 2020)

Manufacturer, LED type	λ_{peak} [nm]	Φ_{e} [mW]	I_{F} [mA]	V_{F} [V]	$2\theta_{1/2}$	Package
Bolb S6060-DR250-W275-P100-V6.5	272	100	250	6.5	150°	6060
Bolb S3535-DR100-W272-P40-V6.5	272	40	100	6.5	160°	3535
Innotek LEUVA66B00HF00	278	3	20	6.5	121°	6060
Innotek LEUVA66G00HF00	278	10	100	7.0	126°	6060
Innotek LEUVA66G00HV00	278	30	350	8.0	120°	6060
Innotek LEUVA66H70HF00	278	70-100	350	8.5	110°	6060
Klaran KL265-50W-SM-WD	260-270	60-80	500	8.0	130°	3535
Lite-On LTPL-G35UV275GC-E	277	10	100	7.2	120°	3535
Lumex SML-LXF3535UVCC10	275	10	100	6.7	120°	3535
Luminus XBT-3535-UV	270-280	40	350	6.5	130°	3535
Nichia NCSU 334B	280	70	350	6.0	115°	6868
Seoul Viosys CUD8AF4D	275	60	600	5.9	120°	6363

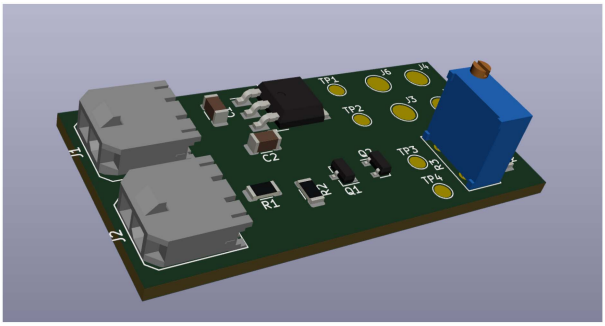

Fig. 8. Layout of the UV LED driver board.

dimming support leads to a tremendous power saving, a factor of 25 in this case. (The gain in terms of power consumption (in Watts) is actually even somewhat larger, since the forward voltage V_{F} reduces as well if the forward current I_{F} of the diode is decreased.) This has a positive effect on the lifetime of the UV LED. Regarding dose rate adjustment, however, there is a tradeoff between minimum irradiation and maximum power consumption.

The custom-made LED driver board supports switching rates of the order of 100 kHz, meaning that the UV LED could be switched ON and OFF about 10^5 times per second. The dc power supply of the driver board can be provided either by a 9–12 V battery or a 9–12 V ac/dc adapter.

3) Pressure Housing Design and Optical Window: Four cylindrical pressure-resistant and UV-resistant reinforced-plastic camera housings were manufactured. Each camera housing, referred to as a dummy, had an outer dimension of 91×270 mm. Fig. 9(a) shows the structure of a camera housing with irradiation from the inside. All four camera housings were equipped with a high-quality uncoated fused silica window (Thorlabs, UV Fused Silica, diameter 50.8 mm, thickness 12 mm, surface flatness Lambda/10, Thorlabs part no. WG42012). According to the datasheet, at 272 nm the transmission coefficient is about 92% at perpendicular incidence. To obtain reproducible results, the UV LED was mounted on a heat sink [see Fig. 9(b)] and placed perpendicular to the center of the optical window, as no camera was installed. The distance between the UV LED and the water-side surface of the window was about 50 mm.

The four dummies were integrated into a metal rack in a parallel arrangement (see Fig. 10). The light beams were not interfering with each other.

III. RESULTS

A. Lab Calibrations

Lab tests in the air were conducted before and after the sea trials. In all irradiance measurements, Optometer X1-1 from Gigahertz-Optik, Germany, was applied.

First, the radiant flux of the selected 272 nm UV LED was measured and compared with the datasheet of the LED. A good agreement within $\pm 5\%$ tolerance was observed regarding the radiant flux Φ_{e} in boresight direction. The square distance law predicted in (6) could be verified, i.e., the received intensity decreases by a factor of four if the distance is doubled in air. For the selected UV LED, the maximum radiant flux occurs at an angle of irradiance of about $\theta = \pm 40°$ with respect to boresight direction due to a build-in lens. If this UV LED is mounted perpendicular to the optical window, this effect is helpful in terms of approximately uniform irradiance along the window, because the larger slant range d_{max} (cf., Figs. 4 and 5) is about compensated by the larger radiant flux in that direction. After the sea trials, no significant degradation of the radiant flux was measured, i.e., the UV LEDs did not alter markedly.

Second, the transmission coefficient of the selected Thorlabs fused silica window was determined. Given $\Phi_{\text{e}} = 40$ mW and assuming perpendicular direction of incidence, immediately behind the optical window an irradiance of $E_{\text{e}} = 480\,\mu\text{W/cm}^2$

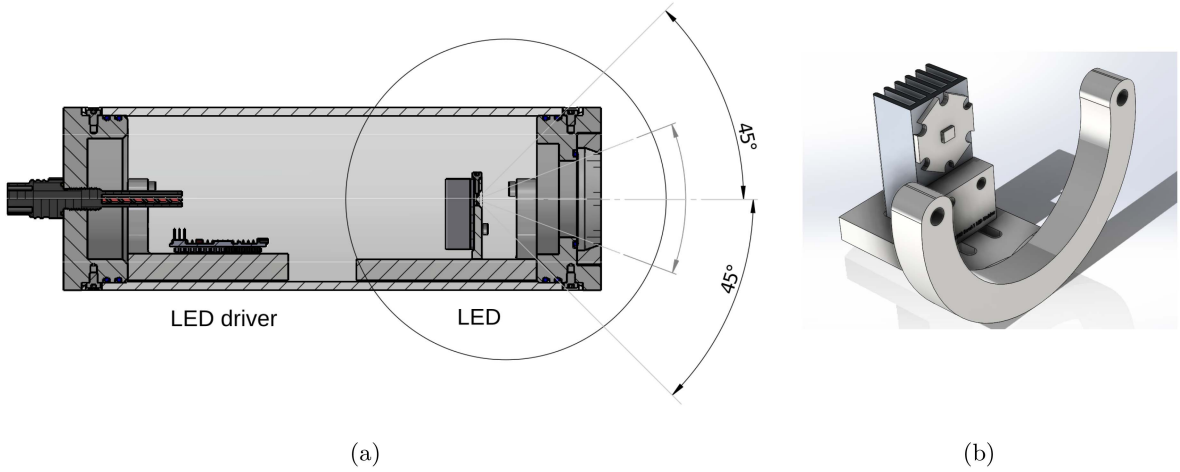

Fig. 9. Housing design: (a) Side view, (b) LED holder. The UV LED is mounted on a heat sink. The distance between LED and optical window is adjustable.

Fig. 10. Rack with four mounted camera housings.

was measured at a distance of 50 mm between UV LED and optometer. Without glass the irradiance was 509 μW/cm^2 at the same distance, cf., (6) and Fig. 6. Hence, the transmission coefficient (as defined above) is about $T_{\mathrm{FS}}(0) = 0.93$ for the selected Thorlabs fused silica window at 272 nm. This value coincides well with the datasheet and with the irradiance analysis in Section II-B. Laboratory measurements were made at a tenfold spacing to reduce measurement errors, and intensities were scaled by a factor of 100 accordingly.

Besides fused silica, also a 80 mm $\times$ 11 mm borosilicate glass was tested in the lab. Given a transmission coefficient of well below 0.01, this type of glass is practically useless at 272 nm.

B. Results of Measurement Campaign

1) Location: Sea tests were carried out from a pontoon of an aquaculture fish farm in Kiel at the eastern side of the Kiel Fjord (GPS coordinates: 54.341422, 10.174099) (see Fig. 1). This location is about 50 m north of the position of the stationary UFO deployed in 2016 and again since 2020. The UV beam direction was facing to the north-east. The rack was attached to the pontoon with two 4 m ropes (see Fig. 10 on right-hand side), thus, the depth was independent of the tidal range. At this location, the average water depth is about 5–6 m. Because of the fish farm, the water is nutrient-rich, and attractive for living organisms.

Fig. 11. Condition in August 2021 at the end of the first measurement period. The two middle camera dummies are D4 (left) and D3 (right). The two outer camera dummies were not illuminated in the summer tests to serve as a benchmark.

2) Measurement Periods: Measurements were carried out in summer and autumn.

a) Measurement period 1: June 16 to August 5, 2021 (50 days).
b) Measurement period 2: August 24 to November 1, 2021 (69 days).

Measurement period 1 is in the peak season from a biofouling perspective, shortly after larvae release. It should not go unmentioned that in northern temperate zones biofouling is very severe in summer. Measurement period 2 falls into the off-season.

3) Irradiation Patterns and Optical Powers: Given the 272 nm 100 mW UV-C LED, different irradiation patterns were tested. In the first measurement period, the following periodic irradiation patterns were chosen.

a) Conventional irradiation pattern (realized in dummy D3): 1 min ON, 9 min OFF.
b) Innovative irradiation pattern 1 (realized in dummy D4): 30 s ON, 30 s OFF, then 30 times 1 s ON, 17 s OFF.

Both irradiation patterns have a duty cycle of 10% (i.e., $\delta = 0.1$) with a period of 10 min, allowing for a fair comparison. In the innovative pattern, the irradiation is more seamless than in the conventional pattern. In the first measurement period, the LED current was limited to $I_\mathrm{F} = 100$ mA in the ON-state. Therefore, the maximum radiant flux of the UV LED was $\Phi_\mathrm{e} = 40$ mW and the irradiance was $E_\mathrm{e} = 480\,\mu$W/cm ^{2} at the water-side surface of the optical window in the ON-state. Given a duty cycle of 10%, the average forward current was 10 mA, the average radiant flux was 4 mW, and the average irradiance was $E_\mathrm{e} = 48\,\mu\mathrm{W/cm}^2$. Any reduction of duty cycle and current reduces the average power consumption and increases the lifetime of the LED, but naturally the dose is also reduced.

The proposed irradiation pattern should not be confused with the low-frequency pulse rates of 0.1–1000 Hz studied in [66] for (nonmarine) biofilm suppression. Such low-frequency pulses result in undesirable averaging of the irradiation.

Because the innovative pattern proved to be advantageous in the first measurement period (see next subsection), this irradiation pattern was further modified in the second measurement period:

a) Innovative irradiation pattern 1 (realized in dummies D2 and D4): 30 s ON, 30 s OFF, then 30 times 1 s ON, 17 s OFF.
b) Innovative irradiation pattern 2 (realized in dummies D1 and D3): 30 times 2 s ON, 18 s OFF.

Innovative pattern 1, as defined in the first measurement phase, now serves as a reference. Innovative pattern 2 also has a duty cycle of 10% and a period of 10 min. Compared to innovative pattern 1, however, the irradiation is more seamless. The ON-time is doubled for most of the time with an almost identical OFF-time. In addition, the LED current was partially limited further: in two dummies it was limited to $I_\mathrm{F} = 50$ mA (this corresponds to a maximum optical power of $\Phi_\mathrm{e} = 20$ mW and an irradiance of $E_\mathrm{e} = 240\,\mu$W/cm ^{2} behind the window in the ON-state), while in the other two dummies it was kept at $I_\mathrm{F} = 100$ mA (corresponding to $E_\mathrm{e} = 480\,\mu\mathrm{W/cm}^2$).

4) Fouling Results: Fig. 11 shows the biofouling results of the first measurement period. The photos were taken at the beginning of August 2021. Biofouling outside the UV light cones was immense. Barnacles dominated, but some mussels also settled. The two outer dummies were not irradiated and used as reference. The windows of the two inner dummies, D3 and D4, were surprisingly clean. A comparison of dummy D4 (innovative irradiation pattern) with dummy D3 (conventional irradiation pattern) shows a clear advantage for the innovative pattern, as can be seen on the right side in Fig. 11. In the case of dummy D4, only a thin biofilm can be seen on the window, despite the seasonally strong biofouling activity. The success rate ("fraction of no settlement") can be estimated as follows.

a) D1 (no irradiation): 0% success rate, window completely overgrown.
b) D2 (no irradiation): 0% success rate, window completely overgrown.
c) D3 (conventional pattern, $E_\mathrm{e} = 480\,\mu\mathrm{W/cm}^2$): 50% success rate, biofilm visible, barnacles, and mussels settle near the edge of the window.
d) D4 (pattern 1, $E_\mathrm{e} = 480\,\mu\mathrm{W/cm}^2$): 70% success rate, thin biofilm, barnacles, and mussels begin to settle near the edge of the window.

Fig. 12. Condition in November 2021 at the end of the second measurement period.

The success rate was evaluated as follows. First, each object that settled on the window was marked with a black foil pen on a transparent foil. Afterward, the transparent area was divided by the total area of the window. Finally, the result was rounded to multiples of 10%.

After the first measurement period, the camera housings, the frame and the cables/ropes were cleaned with citric acid.

Figs. 12 and 13 show the biofouling results of the second measurement period. The photos were taken at the beginning of November 2021. Biofouling, especially by barnacles, was still quite strong during the off-season. Vice versa, only a few mussels settled. Unexpectedly, dummy D3 failed due to a loose cable inside the camera housing. Although not planned, this failure led to the situation that D3 can be used as a reference dummy without irradiation. The success rate ("fraction of no settlement") can be estimated as follows (see Fig. 13).

1) D1 (pattern 2, $E_\mathrm{e} = 240\,\mu\mathrm{W/cm^2}$): 90% success rate, window clean, but biofouling in the area around the optical window.
2) D2 (pattern 1, $E_\mathrm{e} = 240\,\mu\mathrm{W/cm^2}$): 80% success rate, first larvae penetrate from above onto the window (hardly visible in the picture), also biofouling in the area around the window.
3) D3 (pattern 2, $E_\mathrm{e} = 480\,\mu\mathrm{W/cm^2}$ was intended): 30% success rate because of electric failure, strong growth from the edges to the middle of the window.
4) D4 (pattern 1, $E_\mathrm{e} = 480\,\mu\mathrm{W/cm^2}$): 100% success rate, window, and area around window clean.

A comparison between D1 and D2 (same power consumption) indicates that irradiation intervals according to pattern 2 are beneficial. A comparison between D2 and D4 (same irradiation pattern) indicates that the irradiance in D2 is somewhat too small for the given experimental duration.

After the second measurement period, the camera housings, the rack, and the cables/ropes were cleaned again with citric acid.

C. Statistical Analysis

1) Analysis of Variance of the Data: Since the UVC-LED study corresponds to a semiactive experiment in a natural environment (in contrast to a lab experiment), the experimental conditions related to the input data must distinguish between noncontrollable (random) environmental effects (factors) and actively controlled (systematic) technical effects (factors), which are all specified here as X variables in the related statistical analyses. The method of choice for this is the error (or variance) decomposition as part of an ANOVA (analysis of variance) [67], where the experimentally induced variation of the response variable (i.e., output data) is decomposed into an explained (systematic) and a nonexplained (random) part. The nonexplained part is equivalent to the residual variation. The error (or variance) decomposition is also known as "partitioning of the sum of squares." This allows to state how large the total as well as the partial degree of explanation of the experiment and that of the associated individual variables is. Both are expressed in terms of (partial) coefficients of determination (denoted as R^2).

The measured response variable (Y variable) is metrically scaled and is defined here as (inverse) fraction of the gradual colonization progress of the dummy windows (denoted as "fraction of no settlement"). The actively controlled variables include the nominally scaled dummy-based treatment set-up (denoted as "treatment") with the irradiation patterns used in dummies D1, D2, D3, and D4 (see Section III-B3 for details) and the (in principle) metrically scaled UVC irradiance (denoted as "irradiance"), but here realized in the three (ordinal) levels $0\,\mu\mathrm{W/cm^2}$, $240\,\mu\mathrm{W/cm^2}$, and $480\,\mu\mathrm{W/cm^2}$. As the experiment was conducted in two phases (see Section III-B2 for details) in which the measurements were performed under different environmental regimes, another binary scaled random X variable (denoted as "measurement period") with the two phases 1 and 2 was introduced. This X variable stands as a proxy for the (anonymous) effects of the dynamically changing environmental factors during the two experimental periods.

2) Results of the Statistical Analysis: The statistical results of the 3-factor-ANOVA-based error decomposition are reported in Fig. 14. The results indicate that all three factors "treatment," "measurement period," and "irradiance" have a significant effect on the response variable "fraction of no settlement," where the partial degree of explained variation in terms of the partial coefficients of determination R^2 (rounded to the 2nd digit) for "treatment" is 0.20 ($p_\mathrm{F} = 0.0463$, $\alpha = 0.05$) and for "measurement period" and "irradiance" 0.22 ($p_\mathrm{F} = 0.0456$, $\alpha = 0.05$) and 0.56 ($p_\mathrm{F} = 0.0194$, $\alpha = 0.05$), respectively. The total R^2 for the entire experiment is 0.98 ($p_\mathrm{F} = 0.0121$, $\alpha = 0.05$), explaining 98% of the variation induced by the experimental design. Hence, while "irradiance" alone explains 56% of the experimental variation with respect to the gradual colonization progress, the environmental variation in terms of the proxy

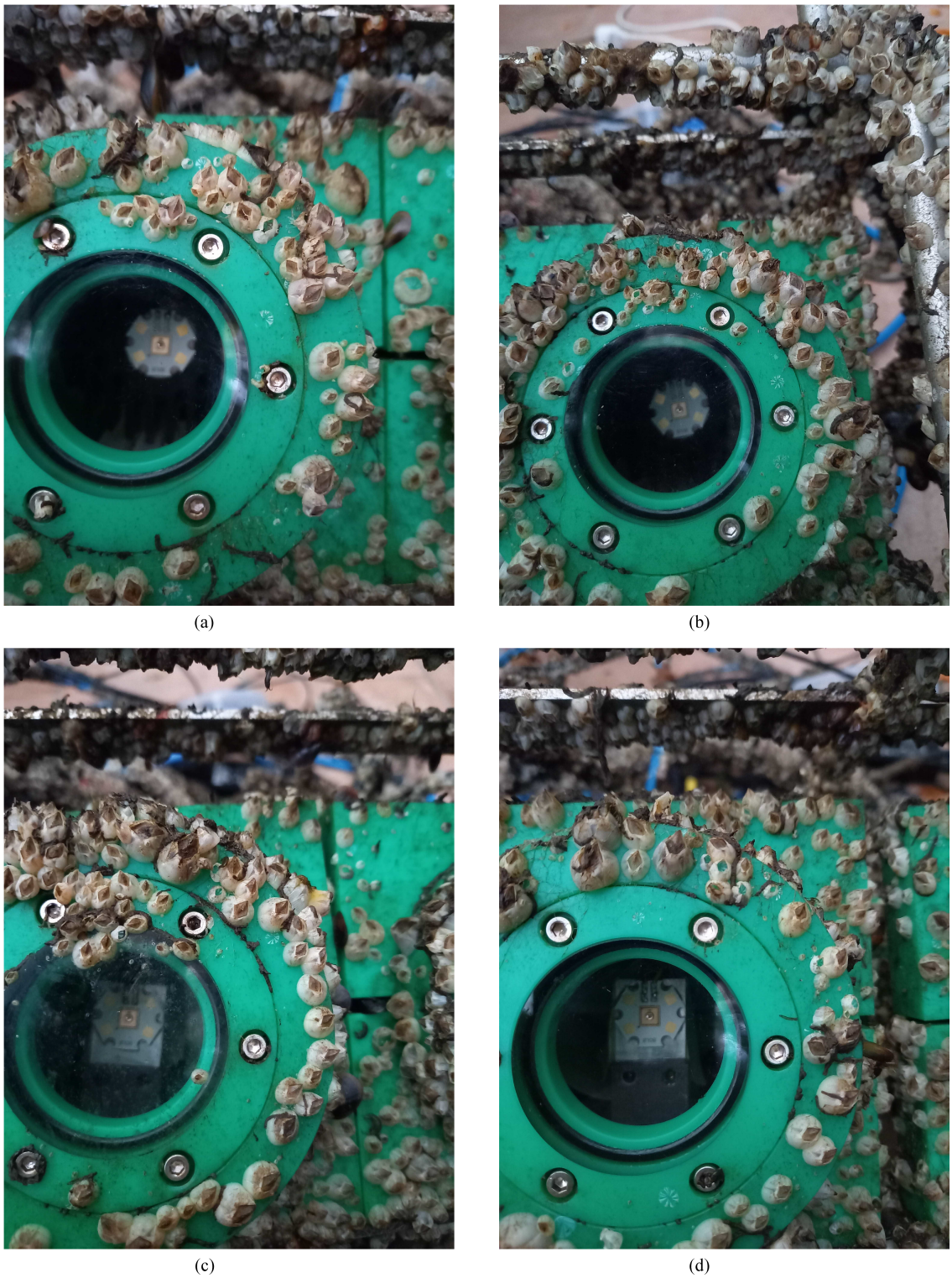

Fig. 13. Condition in November 2021 at the end of the second measurement period (zoom). (a) Camera dummy D1. (b) Camera dummy D2. (c) Camera dummy D3. (d) Camera dummy D4.

"measurement period" explains only 22%. As the ANOVA contains more than one X variable (factor), we used adjusted R^2 values. Both ANOVA restrictions of normal and homoscedastic residuals are also fulfilled (normality: $p_{\text{Anderson-Darling}} > 0.2500$, $\alpha = 0.1$; homoscedasticity: $p_{\text{Levene}} = 0.5745$, $\alpha = 0.1$).

IV. Discussion

Based on the theoretical predictions, investigations and the measurement results, the following observations and recommendations can be formulated.

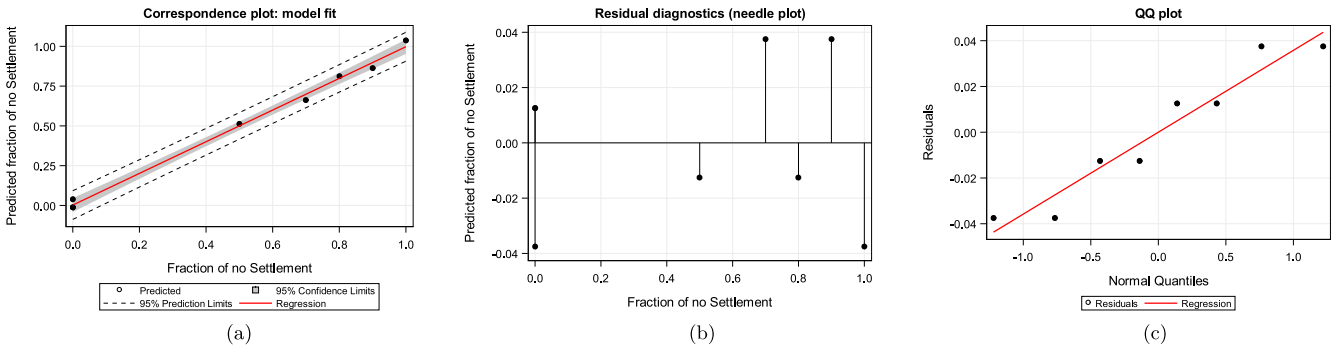

Fig. 14. Generalized linear model (GLM) fit analyzing "fraction of no settlement" as a function of "treatment," "measurement period," and "irradiance" (see text) depicted in a correspondence plot (a). Visual display of the residual diagnostics fulfilling the assumptions of homoscedastic (b) and normal (c) residuals. (a) Correspondence plot. (b) Needle plot. (c) QQ plot.

A. Inside Versus External Irradiation

In the case of underwater cameras and related optical applications, irradiation from the inside of a camera housing is strongly preferable compared to the classical UVC irradiation from the outside. This is due to two reasons: attenuation caused by the water column is completely eliminated and distances can often be reduced, because for both, the internal and external irradiation, the fixtures must be outside the field-of-view of the camera. The radiant flux (and thus, also the electrical power consumption) can be reduced on the order of 100 compared to external irradiation, while still providing approximately the same anti-biofouling effect. Furthermore, a construction employing an internal irradiation device is more compact and has a higher mechanical stability.

B. Irradiance Analysis

The irradiance E_e is derived as a function of the radiant flux Φ_e, the angle of irradiance θ, the directivity $f(\theta)$ of the UV LED, the angle of incidence ϕ, the transmission coefficient $T_{FS}(\phi)$ of the fused silica window, the distance d between UV LED and window, and possibly the attenuation coefficient K of the water column. For UV light, the attenuation is particularly strong compared to common experience with visible light. The dose is proportional to the irradiance, the duty cycle, and the absorption time. The absorption time is a random variable, but for larvae (and other objects with different surface areas and orientations) the irradiance is also randomly distributed.

We believe that mathematical modeling to estimate the UV intensity arriving at the optical window is important for several reasons: 1) to avoid surprises regarding the geometrical arrangement of the irradiation device; 2) to obtain an indication about the necessary power flux and irradiation cycle; 3) to calibrate the irradiation equipment; 4) to document the results of measurement campaigns in a reproducible way. Our analysis is an alternative to ray tracing simulations [46].

C. Irradiation Patterns

The conventional irradiation pattern with relatively long intervals in the 10-min range should be replaced by irradiation with short intervals. With an ON-time of 2 s and an OFF-time of 18 s, for a fixed duty cycle of 10% useful results were achieved. There is a tradeoff between continuous low-intensity irradiation and high-dose irradiation in short pulses. Although the latter case is very effective while the UV LED is switched ON, the time interval in-between pulses may be too long. Larvae that settle on a surface during paused irradiation can hardly be removed by further irradiation. Although continuous irradiation is best from a germicidal point of view, the necessary power consumption is not attractive in mobile and portable devices/systems.

D. Irradiation Intensity

State of the art UVC LEDs have a much shorter lifetime than LEDs in the visible spectral range because commercial manufacturing processes were developed only a few years ago for UVC LEDs. To extend the lifetime, it is recommended to limit the current in the ON-state. With the 100 mW UVC LED used, good results were obtained in the main season at an optical power of 40 mW. 20 mW was sufficient in the off-season. For the setup under investigation, this corresponds to irradiances of $480\,\mu$W/cm^2 and $240\,\mu$W/cm^2 in the ON-state, respectively. On average, given a duty cycle of 10%, the irradiances effectively were $48\,\mu$W/cm^2 and $24\,\mu$W/cm^2, respectively. Care should be taken to ensure heat dissipation of the LED.

E. Electrical Power Consumption

As mentioned in the state-of-the-art section, biofouling mitigation techniques can be classified as passive and active methods. Active methods need an external power supply. In fixed stations and with ships this is typically not a problem, but in mobile and portable devices, power savings are of utmost importance, particularly in long-term sensor deployments. In our campaign, power efficiency has been achieved by several means: Selection of the UVC LED with the largest efficacy available on the market, limitation of the forward current, selection of a small duty cycle, and emphasis on inside irradiation. A positive side effect of these arrangements is a reduction of the aging problem mentioned in [65]. In the sea trials, the peak forward current (in the ON-state) was 50 or 100 mA, respectively. Given a duty cycle of 10%, an average current of 5 or 10 mA was yielded. To calculate the average power consumption, the average current must be multiplied with the power supply voltage. Assuming a 9-V dc

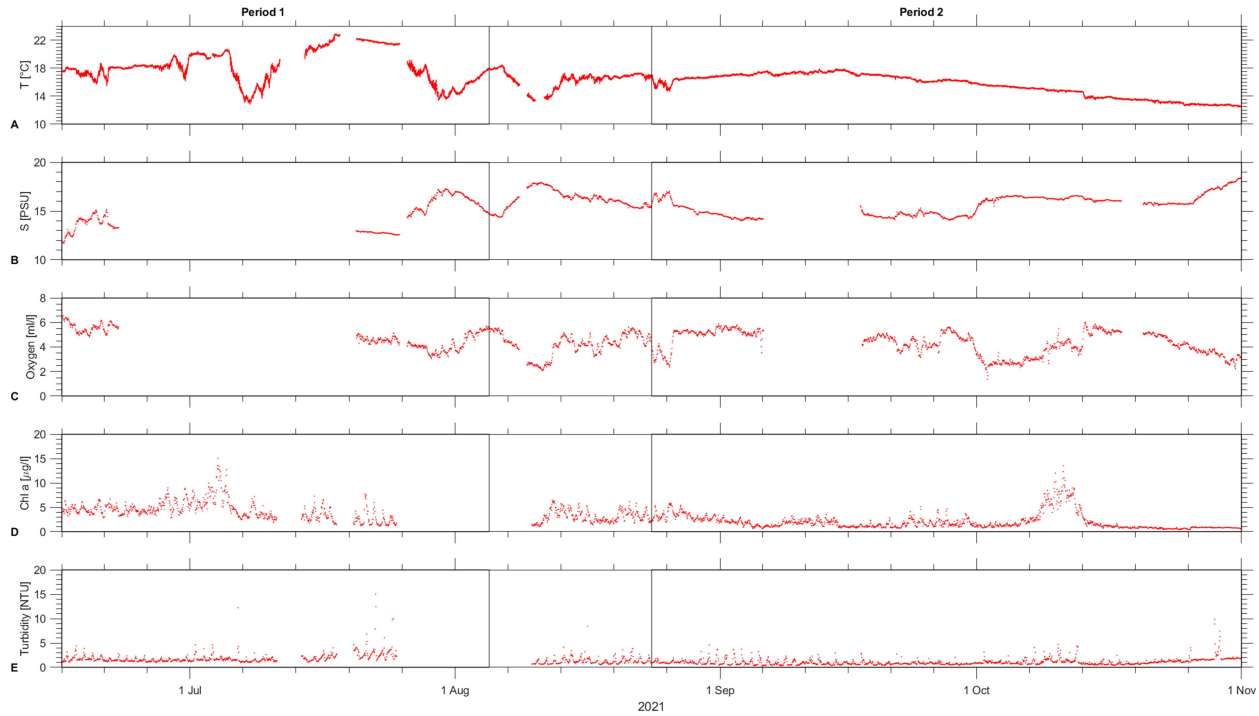

Fig. 15. Abiotic data recorded continuously with different sensors mounted on the adjacent stationary UFO at the study site: water temperature, salinity and oxygen saturation (via a MicroCat-CTD) as well as chlorophyll *a* concentration and turbidity (via an ECO-FL-fluorometer). The presented data are hourly averages for the two experimental periods between June 16 and November 1, 2021.

power supply, the average power consumption is 45 or 90 mW. In this calculation, the power supply of the microcontroller is ignored.

In future work, the efficiency could be further improved by adapting the forward current and/or the duty cycle to biofouling activities. For example, a winter/summer mode and/or a day/night mode is conceivable. On top of this, it is likely that the efficiency of commercial UVC/UVB LEDs will improve in the next years, like they already did for UVA LEDs and for LEDs in the visible range.

F. Mechanical Support

At the site of the measurements under investigation, at a camera depth of 4 m and with the north-eastern orientation, in summer/autumn 2021 there was no noticeable plant grow on the camera windows. In the year before, the situation on the western shore of the Kiel Fjord at 1 m camera depth was quite different, with sea plants growing on deployed samples. A positive influence of UVC light on plant growth could not be determined at that time. In this respect, it is recommended to support the UVC irradiation by a mechanical anti-fouling method, e.g., a wiper or a cleaning robot. Even without coating, glasses can more easily be cleaned mechanically from plant and animal deposits compared to other surfaces (at the risk of scratching, however).

G. Experimental Setting and Environmental Parameters

The statistical analysis in Section III-C revealed the factor "measurement period" to be of less importance when compared to the factors "treatment" and "irradiance." We emphasize here again, that due to different scaling of the individual environmental parameters reflected in the factor "measurement period," the experimental design did not allow for an inclusion into the analysis and that we therefore present these data only descriptively. Visual inspections of the camera housings indicated nearly complete coverage of the nonirradiated structures by fouling organisms after the end of both experimental periods (Figs. 11–13).

Lastly, we present descriptively the time series of parallel measured abiotic factors such as temperature, salinity, chlorophyll *a*, and turbidity (see Fig. 15), and discuss in light of the current literature which of these factors may have most favored biofouling. The first measurement period reflects very well the summer warming of the Kiel Fjord, which was interrupted by two cold periods: water temperature was about 17.5 °C at the beginning in June 2021, reached up to 22.8 °C in mid-July 2021, and dropped to about 12.5 °C at the end of the experiment in early November 2021. The course of the salinity data during the two experimental phases reflects the exact opposite trend of the temperature data, which can be seen particularly clearly between mid-June and the end of July. From mid-September to the end of the second measurement period, the water temperature decreases continuously. The observed daily and seasonal variability in temperature and salinity in the Baltic Sea, result from the inflow of salty water masses from the North Sea and river discharge, as well as daily insolation and heat exchange with the atmosphere, leading to the formation of variable thermohaline stratification [68]. Nasrolahi et al. [7], [8] investigated interacting effects of temperature and salinity on early life performance and settlement of *B. improvisus* in the Baltic Sea. The authors revealed overall warming water temperatures (with a maximum

of 28 °C) to increase survival, accelerate larval development and metamorphosis to cyprids, and thus, increase the overall settlement of larvae on prevailing surfaces. In contrast, high salinities (of 30 PSU) revealed lowest settlement rates, whereas intermediate salinities (of approximately 15 PSU) allowed for highest rates. The increasing temperature at our study site, especially in the first experimental phase, as well as the intermediate salinities between 12 and 15 PSU in the first days of that phase may have contributed to the increased settlement rates of *B. improvisus* on the surfaces of the experimental set-up, and well reflect the findings of the authors mentioned above. Increased amounts of measured chlorophyll *a* indicate high availability of food sources—not only for the filter feeding barnacles, but also for secondary settlers, such as *M. edulis*. The latter have been shown to prosper with increasing ingestion and growth rates through increasing algal concentrations [69]. The same effect was seen with increased suspended bottom material. In the case of the fish farm, from which the set-up was deployed, however, the suspension of organic and/or suspended bottom material was very low and turbidity measurements did not exceed an average of 5 (NTU). Apart from available food sources, the actual settlement of *M. edulis* is, in addition to other factors, dependent upon the presence of epibionts (here, for example, the barnacles) to attach byssus threads in the first place [70]. In our case, this may have contributed to a rapid attachment and further colonization of mussels.

V. Conclusion

The focus of this article was on UVC-LED-based biofouling suppression for underwater cameras, besides other optical instrumentation. Emphasis was on UVC irradiation from the inside of a pressure housing into the water column. This configuration avoids attenuation by the water column, which is particularly strong in the UVC regime. The irradiance was analyzed and compared for internal and external UV irradiation configurations. Shorter periodic irradiation intervals, more seamless than those commonly used, have been proposed to reduce the electrical power consumption while maintaining biofouling control. Experimental verification was performed in the urban Kiel Fjord, located in the southwest Baltic Sea, as part of the UFOTriNet long-term fish monitoring project. The results of the measurement campaign were supported by an ANOVA-based statistical analysis.

Acknowledgment

The authors would like to thank Y. Rößner and S. Bodenstein (Aquakulturgesellschaft Ostseeforelle, Kiel, Germany) for their support of the UFOTriNet project by providing access to the electrical grid, accommodations for the electronic equipment, and assistance with deployment and recovery of the UFO and the experimental equipment.

References

[1] S. M. Bilodeau, A. W. H. Schwartz, B. Xu, V. P. Pauca, and M. R. Silman, "A low-cost, long-term underwater camera trap network coupled with deep residual learning image analysis," *PLoS One*, vol. 17, 2022, Art. no. 0263377, doi: 10.1371/journal.pone.0263377.

[2] J. Li et al., "Development of a buoy-borne underwater imaging system for in situ mesoplankton monitoring of coastal waters," *IEEE J. Ocean. Eng.*, vol. 47, no. 1, pp. 88–110, Jan. 2022, doi: 10.1109/JOE.2021.3106122.

[3] P. A. Hoeher, J. Sticklus, and A. Harlakin, "Underwater optical wireless communications in swarm robotics: A tutorial," *IEEE Commun. Surv. Tut.*, vol. 23, no. 4, pp. 2630–2659, Fourthquarter 2021, doi: 10.1109/COMST.2021.3111984.

[4] M. Wahl, "Marine epibiosis. I. Fouling and antifouling: Some basic aspects," *Mar. Ecol. Progr. Ser.*, vol. 58, pp. 175–189, 1989.

[5] S. Dürr and M. Wahl, "Isolated and combined impacts of bluemussels (Mytilus edulis) and barnacles (Balanus improvisus) on structure and diversity of a fouling community," *J. Exp. Mar. Biol. Ecol.*, vol. 306, pp. 181–195, 2004, doi: 10.1016/j.jembe.2004.01.006.

[6] A. Wallin, S. Qvarfordt, P. Norling, and H. Kautsky, "Benthic communities in relation to wave exposure and spatial positions on sublittoral boulders in the Baltic Sea," *Aquat Biol.*, vol. 12, pp. 119–128, 2011, doi: 10.3354/ab00329.

[7] A. Nasrolahi, C. Pansch, M. Lenz, and M. Wahl, "Temperature and salinity interactively impact early juvenile development: A bottleneck in barnacle ontogeny," *Mar. Biol.*, vol. 160, pp. 1109–1117, 2013, doi: 10.1007/s00227-012-2162-8.

[8] A. Nasrolahi, J. Havenhand, A.-L. Wrange, and C. Pansch, "Population and life-stage specific sensitivities to temperature and salinity stress in barnacles," *Sci. Rep.*, vol. 6, pp. 1–10, 2016, doi: 10.1038/srep32263.

[9] C. Bueley, D. Olender, and B. Bocking, "In-situ trial of UV-C as an antifoulant to reduce biofouling induced measurement error," *J. Ocean. Technol.*, vol. 9, no. 4, pp. 48–67, 2014.

[10] W. Kowalski, *Ultraviolet Germicidal Irradiation Handbook*. Heidelberg, Germany: Springer, 2009.

[11] L. Tian, Y. Yin, W. Bing, and E. Jin, "Antifouling technology trends in marine environmental protection," *J. Bionic. Eng.*, vol. 18, pp. 239–263, 2021, doi: 10.1007/s42235-021-0017-z.

[12] A. Delgado, C. Briciu-Burghina, and F. Regan, "Antifouling strategies for sensors used in water monitoring: Review and future perspectives," *Sensors*, vol. 21, 2021, Art. no. 389, doi: 10.3390/s21020389.

[13] D. Laurent, C. Chantal, and L. Michel, "Biofouling protection for marine environmental sensors," *Ocean. Sci.*, vol. 6, no. 2, pp. 503–511, 2010, doi: 10.5194/os-6-503-2010.

[14] H. Lobe, "Recent advances in biofouling protection for oceanographic instrumentation," in *Proc. IEEE/MTS OCEANS*, Washington, DC, USA, 2015, pp. 1–4.

[15] J. Joslin and B. Polagye, "Demonstration of biofouling mitigation methods for long-term deployments of optical cameras," *Mar. Technol. Soc. J.*, vol. 49, pp. 88–96, 2015, doi: 10.4031/MTSJ.49.1.12.

[16] C. Li et al., "Analysis of removing barnacles attached on rough substrate with cleaning robot," *J. Mar. Sci. Eng.*, vol. 8, 2020, Art. no. 569, doi: 10.3390/jmse8080569.

[17] S. McLean, B. Schofield, G. Zibordi, M. Lewis, S. Hooker, and A. Weidemann, "Field evaluation of antibiofouling compounds on optical instrumentation," *Proc. SPIE*, vol. 2963, pp. 708–713, 1997, doi: 10.1117/12.266389.

[18] D. M. Yebra, S. Kiil, and K. Dam-Johansen, "Antifouling technology–past, present and future steps towards efficient and environmentally friendly antifouling coatings," *Prog. Org. Coatings*, vol. 50, pp. 75–104, 2004, doi: 10.1016/j.porgcoat.2003.06.001.

[19] H. Lobe and A. Das, "The ClearSignal biofouling control system for oceanographic instrumentation," in *Proc. IEEE/MTS OCEANS*, Seattle, WA, USA, 2010, pp. 1–2.

[20] I. Hoelken, M. Hoppe, Y. K. Mishra, S. N. Gorb, R. Adelung, and M. J. Baum, "Complex shaped ZnO nano- and microstructure based polymer composites: Mechanically stable and environmentally friendly coatings for potential antifouling applications," *Phys. Chem. Chem. Phys.*, vol. 18, no. 10, pp. 7114–7123, 2016, doi: 10.1039/C5CP07451G.

[21] H. Qiu, "Functional nanomaterials for environmentally friendly biofouling control," Ph.D. dissertation, Faculty Eng., Kiel Univ., Kiel, Germany, 2022.

[22] D. S. Petersen, T. Kleinteich, S. N. Gorb, and L. Heepe, "Competing with barnacle cement: Wetting resistance of a re-entrant surface reduces underwater adhesion of barnacles," *J. Roy. Soc. Interface*, vol. 15, 2018, Art. no. 20180396, doi: 10.1098/rsif.2018.0396.

[23] C. Tendero et al., "Nanocomposite thin film of Ag nanoparticles embedded in amorphous Al $_2$ O$_3$ on optical sensors windows: Synthesis, characterization and targeted application towards transparency and anti-biofouling," *Surf. Coatings Technol.*, vol. 328, pp. 371–377, 2017, doi: 10.1016/j.surfcoat.2017.08.061.

[24] P. Wang, D. Zhang, S. Sun, T. Li, and Y. Sun, "Fabrication of slippery lubricant-infused porous surface with high underwater transparency for the control of marine biofouling," *Appl. Mater. Interfaces*, vol. 9, pp. 972–982, 2017, doi: 10.1021/acsami.6b09117.

[25] L. Delauney and C. Compere, "An example: Biofouling protection for marine environmental sensors by local chlorination," in *Marine and Industrial Biofouling*, H.-C. Flemming, P. S. Murthy, R. Venkatesan, and K. Cooksey Eds., Berlin, Germany:Springer, 2009.

[26] S. Zhang, J. Xi, J. Wu, P. Wang, F. Lin, and D. Zhang, "Design of an efficient antifouling strategy for underwater optical window based on chlorine generation," *Colloids Surf. A: Physicochem. Eng. Aspects*, vol. 634, 2022, Art. no. 127922, doi: 10.1016/j.colsurfa.2021.127922.

[27] D. V. Manov, G. C. Chang, and T. D. Dickey, "Methods for reducing biofouling of moored optical sensors," *J. Atmos. Ocean. Technol.*, vol. 21, pp. 958–968, 2004, doi: 10.1175/1520-0426(2004)021<0958:MFRBOM>2.0.CO;2.

[28] S. F. Guo et al., "Effect of ultrasound on cyprids and juvenile barnacles," *Biofouling*, vol. 27, pp. 185–192, 2011, doi: 10.1080/08927014.2010.551535.

[29] M. Salta, L. R. Goodes, B. J. Maas, S. P. Dennington, T. J. Secker, and T. G. Leighton, "Bubbles versus biofilms: A novel method for the removal of marine biofilms attached on antifouling coatings using ultrasonically activated water stream," *Surf. Topogr. Metrol. Properties*, vol. 4, pp. 1–10, 2016, doi: 10.5258/SOTON/399420.

[30] L. Zheng, Y. Zeng, Y. Li, and J. Zheng, "Study on the application of ultrasonic wave in the removal of mcirofouling on PMMA surface," *Biosurface Biotribol.*, vol. 7, pp. 119–125, 2021, doi: 10.1049/bsb2.12014.

[31] V. Naddeo, A. Cesaro, D. Mantzavinos, D. Fatta-Kassinos, and V. Belgiorno, "Water and wastewater disinfection by ultrasound irradiation - A critical review," *Glob. Nest. J.*, vol. 16, no. 3, pp. 561–577, 2014.

[32] Y. Li and C. Ning, "Latest research progress of marine microbiological corrosion and bio-fouling, and new approaches of marine anti-corrosion and anti-fouling," *Bioactive Mater.*, vol. 4, pp. 189–195, 2019, doi: 10.1016/j.bioactmat.2019.04.003.

[33] J. Schwarze et al., "Reduction of biofilm accumulation by constant and alternating potentials in static and dynamic field experiments," *Biofouling*, vol. 38, pp. 119–130, 2022, doi: 10.1080/08927014.2022.2027923.

[34] Z. Tian, Z. Lei, X. Chen, and Y. Chen, "Evaluation of laser cleaning for defouling of marine biofilm contamination on aluminum alloys," *Appl. Surf. Sci.*, vol. 499, 2020, Art. no. 144060, doi: 10.1016/j.apsusc.2019.144060.

[35] H. K. Lotze, B. Worm, M. Molis, and M. Wahl, "Effects of UV radiation and consumers on recruitment and succession of a marine macrobenthic community," *Mar. Ecol. Progr. Ser.*, vol. 243, pp. 57–66, 2002, doi: 10.3354/meps243057.

[36] W. L. Chiang, D. W. T. Au, P. K. N. Yu, and R. S. S. Wu, "UV-B damages eyes of barnacle larvae and impairs their photoresponses and settlement success," *Environ. Sci. Technol*, vol. 37, no. 6, pp. 1089–1092, 2003, doi: 10.1021/es0261168.

[37] O. S. Hung, L. A. Gosselin, V. Thiyagarajan, R. S. S. Wu, and P. Y. Qian, "Do effects of ultraviolet radiation on microbial films have indirect effects on larval attachment of the barnacle balanus amphitrite?," *J. Exp. Mar. Biol. Ecol.*, vol. 323, no. 1, pp. 16–26, 2005, doi: 10.1016/j.jembe.2005.02.016.

[38] W. L. Chiang, R. S. S. Wu, P. K. N. Yu, and D. W. T. Au, "Are barnacle larvae able to escape from the threat of UV?," *Mar. Biol.*, vol. 151, pp. 703–711, 2007, doi: 10.1007/s00227-006-0508-9.

[39] P. V. Perepelizin and D. Boltovskoy, "Effects of 254 nm UV irradiation on the mobility and survival of larvae of the invasive fouling mussel Limnoperna fortunei," *Biofouling*, vol. 30, pp. 197–202, 2014, doi: 10.1080/08927014.2013.855726.

[40] P. H. Benson, D. L. Brining, and D. W. Perrin, "Marine fouling and its prevention," *Mar. Technol.*, vol. 10, pp. 30–37, 1973.

[41] L. H. DiSalvo and A. B. Cobet, "Control of an estuarine microfouling sequence on optical surfaces using low-intensity ultraviolet irradiation," *Appl. Microbiol.*, vol. 27, no. 1, pp. 172–178, 1974.

[42] A. Lakretz, E. Z. Ron, and H. Mamane, "Biofouling control in water by various UVC wavelengths and doses," *Biofouling*, vol. 26, no. 3, pp. 257–267, 2010, doi: 10.1080/08927010903484154.

[43] J. S. Patil, H. Kimoto, T. Kimoto, and T. Saino, "Ultraviolet radiation (UV-C): A potential tool for the control of biofouling on marine optical instruments," *Biofouling*, vol. 23, no. 4, pp. 215–230, 2007, doi: 10.1080/08927010701275598.

[44] M. Berney, H. U. Weilenmann, and T. Egli, "Adaptation to UVA radiation of E. Coli growing in continuous culture," *J. Photochem. Photobiol.*, vol. 86, pp. 149–159, 2007.

[45] A. Hamamoto et al., "New water disinfection system using UVA light-emitting diodes," *J. Appl. Microbiol.*, vol. 103, pp. 2291–2298, 2007.

[46] B. Salters and R. Piola, "UVC light for antifouling," *Mar. Technol. Soc. J.*, vol. 51, no. 2, pp. 59–70, 2017, doi: 10.4031/MTSJ.51.2.10.

[47] K. Z. Hunsucker et al., "Using ultraviolet light for improved antifouling performance on ship hull coatings," *Biofouling*, vol. 35, no. 6, pp. 58–668, 2019, doi: 10.1080/08927014.2019.1642334.

[48] A. F. MacKenzie, E. A. Maltby, N. Harper, C. Bueley, D. Olender, and R. C. Wyeth, "Periodic ultraviolet-c illumination for marine sensor antifouling," *Biofouling*, vol. 35, no. 5, pp. 483–493, 2019, doi: 10.1080/08927014.2019.1616698.

[49] E. Ryan, S. Turkmen, and S. Benson, "An investigation into the application and practical use of (UV) ultraviolet light technology for marine antifouling," *Ocean. Eng.*, vol. 216, 2020, doi: 10.1016/j.oceaneng.2020.107690.

[50] C. Braga, K. Hunsucker, H. Gardner, and G. Swain, "A novel design to investigate the impacts of UV exposure on marine biofouling," *Appl. Ocean. Res.*, vol. 101, 2020, Art. no. 102226, doi: 10.1016/j.apor.2020.102226.

[51] K. N. Richard, K. Z. Hunsucker, H. Gardner, K. Hickman, and G. Swain, "The application of UVC used in synergy with surface material to prevent marine biofouling," *J. Mar. Sci. Eng.*, vol. 9, 2021, Art. no. 662, doi: 10.3390/jmse9060662.

[52] P. Whitworth, N. Aldred, K. J. Reynolds, J. Plummer, P. W. Duke, and A. S. Clare, "Importance of duration, duty-cycling and thresholds for the implementation of ultraviolet C in marine biofouling control," *Front. Mar. Sci.*, vol. 8, 2022, Art. no. 809011, doi: 10.3389/fmars.2021.809011.

[53] J. M. Titus and B. S. Ryskiewich, "Ultraviolet marine anti-biofouling systems," U.S. Patent 5 322 569 A, 1994.

[54] N. E. Farr, C. T. Pontbriand, and T. G. Peters, "Marine environment antifouling system and methods," U.S. Patent 9 235 048 B2, 2016.

[55] J. Sticklus, T. Kwasnitschka, and P. A. Hoeher, "Method and device for potting an LED luminaire potted in a potting compound, and LED luminaire," U.S. Patent 2017/0 334 114 A1, 2017.

[56] B. A. Salters, "System for anti-biofouling," U.S. Patent 2018/0 001 356 A1, 2018.

[57] J. J. Leijssen, "Method and system for protecting a surface against biofouling," U.S. Patent 2021/0 348 753 A1, 2021.

[58] J. Zouak, "UV.Xchange biofouling control: Any surface, foul free," *Eco*, pp. 48–49, 2014.

[59] Leibniz Institute for Baltic Sea Research (IOW), "Innovatives antifouling-system für serienproduktion lizensiert," *Schiff Hafen*, vol. 10, pp. 34–35, 2021.

[60] R. Kitamura, L. Pilon, and M. Jonasz, "Optical constants of silica glass from extreme ultraviolet to far infrared at near room temperature," *Appl. Opt.*, vol. 46, no. 33, pp. 8118–8133, 2007, doi: 10.1364/AO.46.008118.

[61] P. Kowalczuk, J. Olszewski, M. Darecki, and S. Kaczmarek, "Empirical relationships between coloured dissolved organic matter (CDOM) absorption and apparent optical properties in baltic sea waters," *Int. J. Remote Sens.*, vol. 26, pp. 345–370, 2005, doi: 10.1080/01431160410001720270.

[62] M. Tedetti and R. Sempere, "Penetration of ultraviolet radiation in the marine environment. A review," *Photochem. Photobiol.*, vol. 82, pp. 389–397, 2006, doi: 10.1562/2005-11-09-IR-733.

[63] A. M. Gretarsson, *A First Course in Laboratory Optics*. Cambridge, U.K.: Cambridge Univ. Press, 2021.

[64] J. L. Davis et al., "Initial benchmarks of UV LEDs and comparisons with white LEDs," U.S. Department of Energy-Lighting R&D Program, vol. DOE/EE-2543, Nov. 2021.

[65] T.-C. Hsu et al., "Perspectives on UVC LED: Its progress and application," *Photon. 2021*, vol. 8, 2021, Art. no. 196, doi: 10.3390/photonics8060196.

[66] J. Li, K. Hirota, H. Yumoto, T. Matsuo, Y. Miyake, and T. Ichikawa, "Enhanced germicidal effects of pulsed UV-LED irradiation on biofilms," *J. Appl. Microbiol.*, vol. 109, pp. 2183–2190, 2010, doi: 10.1111/j.1365-2672.2010.04850.x.

[67] B. G. Tabachnick and L. S. Fidell, *Experimental Designs Using ANOVA*. Belmont, CA, USA: Duxbury, 2007.

[68] A. Lehmann and H. H. Hinrichsen, "On the thermohaline variability of the baltic sea," *J. Mar. Syst.*, vol. 25, pp. 333–357, 2000, doi: 10.1016/S0924-7963(00)00026-9.

[69] T. Kiørboe, F. Møhlenberg, and O. Nøhr, "Effect of suspended bottom material on growth and energetics in mytilus edulis," *Mar. Biol.*, vol. 61, pp. 283–288, 1981, doi: 10.1007/BF00401567.

[70] Y. L. Garner and M. K. Litvaitis, "Effects of wave exposure, temperature and epibiont fouling on byssal thread production and growth in the blue mussel, Mytilus edulis, in the Gulf of Maine," *J. Exp. Mar. Biol. Ecol.*, vol. 446, pp. 52–56, 2013, doi: 10.1016/j.jembe.2013.05.001.

Peter Adam Hoeher (Fellow, IEEE) received the Dipl.Ing. (M.Sc.) degree from RWTH Aachen University, Aachen, Germany, in 1986, and the Dr.Ing. (Ph.D.) degree from the University of Kaiserslautern, Kaiserslautern, Germany, in 1990, both in electrical engineering.

From 1986 to 1998, he was with the German Aerospace Center (DLR), Oberpfaffenhofen, Germany. From 1991 to 1992, he was on leave with AT&T Bell Laboratories, Murray Hill, NJ, USA. Since 1998, he has been a Full Professor of Electrical and Information Engineering with Kiel University, Kiel, Germany. His research interests include wireless communications, including underwater optical wireless communication and optical biofouling mitigation.

Oliver Zenk graduated in mechanical engineering from the University of Applied Sciences, Kiel, Germany, in 2002.

He is currently a Senior Design Engineer with MacArtney Germany, Kiel. In 2004, after being introduced to subsea technology during an internship semester with Webb Research Cooperation, he was with Optimare Marine Messsysteme GmbH and Co.KG, Bremerhaven, Germany, building autonomous submergible ice drifters for the Alfred Wegener Institute, Bremerhaven, Germany. From 2014–2018, he was with MacArtney Germany and has been there again since 2021. Among many other projects, he was responsible for the design of the stationary underwater fish observatory as well as the UVC testbed.

Boris Cisewski received the Diploma from the Christian Albrechts University Kiel, Germany, in 1995, and the Ph.D. degree (Dr.rer.nat.) from the Faculty 1 Physics/Electrical Engineering, University of Bremen, Bremen, Germany, in 2000, both in physical oceanography.

He currently leads the research unit Operational Observation Systems with the Thuenen Institute of Sea Fisheries, Bremerhaven, Germany. His main scientific interests include the physical oceanography of the North Atlantic and the Arctic Ocean, investigation on the influence of physical processes on fish stocks and marine ecosystems in the North Atlantic and Arctic Ocean, and the development of noninvasive optic/acoustic measuring methods and new measuring strategies for the monitoring of fish stocks and marine ecosystems.

Karin Boos received the graduation degree in biology and the Ph.D. degree in bioinvasions in the marine realm from Freie Universität, Berlin, Germany, in 2004 and 2009, respectively.

Having thereafter worked in consultancy (bird-migration and offshore windfarms, Germany, 2010–2014), the University of Bremen, Bremen, Germany (research in ophiuroid ecology), and the graduate school GLOMAR with the Center for Marine Environmental Sciences (MARUM, both 2014–2019). She has been working as a Project Manager with the Thuenen Institute of Sea Fisheries, Bremerhaven, Germany, since 2019.

Joachim Groeger received the diploma (M.Sc.) in biology and computer sciences, and Dr.rer.nat (Ph.D.) degrees in fishery biology, statistics, and computer sciences from Kiel University, Kiel, Germany, in 1987 and 1992, respectively, the Habilitation degree in zoology from Rostock University, Rostock, Germany, in 2002, and the Habilitation degree in fisheries biology from Kiel University in 2006. He has studied biology (marine biology, fishery biology, zoology), computer science, statistics, and econometrics from Kiel University and the Institute for Marine Sciences (IfM), Kiel, Germany.

He has been a Scientific Employee with the IfM, Kiel University, a Systems Analyst with a software company in Hamburg, Germany, a Scientist with the Institute for Baltic Sea Fishery, Rostock, Germany, an Associate Professor for Zoology with the University of Rostock (in parallel), a Professor of Fishery Oceanography with the University of Massachusetts, Boston, MA, USA, a Scientific Director with the Thuenen Institute of Sea Fisheries in Hamburg/Bremerhaven, a Professor in Fisheries Biology with the University of Rostock (in parallel), and a Principal Investigator, University Lecturer and Guest Professor with GEOMAR Helmholtz Centre for Ocean Research Kiel (in parallel). He retired in November 2022.